Koopman-based data-driven control for continuous fluidized bed spray granulation

Anton Maksakov [*] Stefan Palis[*, **]

[*] *Otto-von-Guericke University, D-39106 Magdeburg, Germany*
[**] *National Research University "Moscow Power Engineering Institute", Moscow, Russia*

Abstract: Continuous fluidized bed spray granulation processes are known to be prone to non-linear oscillations, which requires a stabilizing controller design. In this article, a purely data-driven Koopman-based system linearization and control is proposed, which does not need any prior model knowledge and uses only systems input-output measurements. The linearization achieved by the Koopman embedding allows for linear-quadratic control design, which does not depend on the operating point. The proposed method was validated in a simulation study of a fluidized bed granulation process and was able to stabilize the particle size distribution in different operating points.

Keywords: Granulation, fluidized bed, neural networks, Koopman embedding, data-based control

1. INTRODUCTION

Fluidized bed spray granulation (FBSG) processes allow for generation of dust-less and free-flowing particles of desired dimensions. Thus, it is widely used in chemical, pharmaceutical, and food industries. Despite its importance, the dynamical properties of the process are often not fully understood and the controller design remains a challenging task. Different solutions were proposed, like linear model predictive control (Bück et al. (2016)), robust H_∞ loop-shaping (Palis and Kienle (2012b)) or nonlinear discrepancy based control (Palis and Kienle (2012a, 2014). These approaches heavily depend on model accuracy and are designed for a narrow band of operational regimes. However, the dynamics of the fluidized bed spray granulation is strongly dependent on the process conditions and thus typically time-varying and modeled with considerable uncertainties.

Recently, a data-driven Koopman operator based approach is emerging in modeling and control theory (Brunton et al. (2016), Mauroy et al. (2020)). The idea here is to lift the original states of a nonlinear system up to higher-dimensional embedded coordinates, where the dynamics of the system is approximately linear. It has shown successful results in different fields, like mechanical and fluid dynamics (Lusch et al. (2018)), chemical processes (Narasingam and Kwon (2019)), power electronics (Maksakov and Palis (2020)) and others.

In this paper, a data-driven Koopman based approach is proposed for a global linearization of the fluidized bed spray granulation process. It does not require model knowledge and can be used with partially measured states. To discover the higher-dimensional embedding a deep neural network is used. The resulting linear representation of the system allows for the use of linear control theory for controller design, like linear quadratic (LQ) optimal

control (Brunton et al. (2016), Kaiser et al. (2017)) or linear model predictive control (Korda and Mezić (2018)). The paper is organized as follows: in section 2 the model of continuous bed spray granulation with internal product classification is introduced. In section 3 the method of data-driven identification of the Koopman-invariant subspace is given. Further, in section 4, a linear quadratic controller is designed based on the identified linearized system. Lastly, the performance of the proposed method is shown using numerical simulations.

2. FLUIDIZED BED SPRAY GRANULATION

The granulator consists of a granulation chamber, an injection nozzle, and a tube for particle withdrawal as shown in Fig.1. The chamber contains a large number of particles, which are constantly fluidized by an upstream flow of heated gas. The injection nozzle sprays a suspension or a solution to the main chamber, which moisturizes the granules. After drying the injected liquid leads to the growth of the particles. In addition, part of the injected liquid results in the generation of new nuclei. The withdrawal tube in the lower part of the chamber provides an internal classification of the product with an adjustable counter-current gas flow. This classification flow sets the minimal size of the particles, which are withdrawn from the granulator, where the smaller particles are blown back to the main chamber. The described process configuration can be described by population balance modeling (Randolph and Larson (1971), Vreman et al. (2009)), which leads to the following equation

$$\frac{\partial n}{\partial t} = -G\frac{\partial n}{\partial L} - \dot{n}_{prod} + \dot{n}_{nuc}. \tag{1}$$

Here, the first term describes the growth of the particles, the second term accounts for product withdrawal, and the last term is related to the generation of new particles.
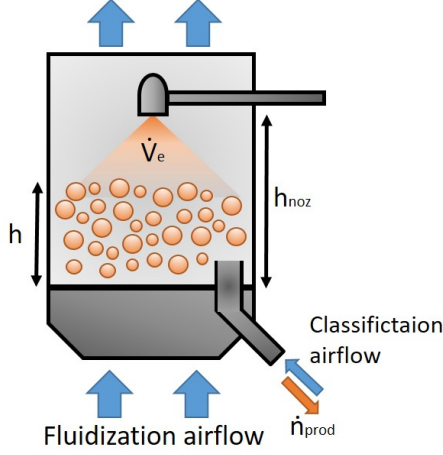
Fig. 1. Process scheme.

According to Vreman et al. (2009), the growth rate of the particles depends on the injection rate $\dot{V}_e$, where the part of injected liquid proportional to $(1 - b)$ contributes to the growth, and another part, which is proportional to b, contributes to the generation of new nuclei. The growth rate G is given as:

$$G = \frac{2(1 - b)\dot{V}_e}{\pi \mu_2},$$ (2)

where μ_2 stands for the second moment of the distribution and can be calculated as follows:

$$\mu_2 = \int_0^\infty L^2 n dL.$$ (3)

Droplets, which do not settle on the particles, get dried by the heated airflow and create new nuclei. Here, it is assumed, that the generation of new particles is normally distributed with a medium diameter L_0 and deviation σ_0

$$\dot{n}_{nuc} = \frac{b\dot{V}_e}{\frac{1}{6}\pi} \delta(L_0, \sigma_0),$$ (4)

where $\delta(L_0, \sigma_0)$ is a normal distribution normalized with its third moment:

$$\delta(L) = \frac{exp(-\frac{(L - L_0)^2}{\sigma_0})}{\int_0^\infty L^3 exp(-\frac{(L - L_0)^2}{\sigma_0}) dL}.$$ (5)

The proportionality factor b depends on the distance between the particle bed and the injection nozzle. According to Vreman et al. (2009), it is assumed to have a linear dependence, which is limited with a minimum value b_∞ and maximum value of $b = 1$:

$$b = b_\infty + max\left(0, (1 - b_\infty)\frac{h_{noz} - h}{h_{noz}}\right).$$ (6)

Here, h_{noz} is the height of the nozzle and h is the height of the bed, which can be calculated from its volume V assuming a constant bed porosity ε and using the cross-sectional area of the main chamber A.

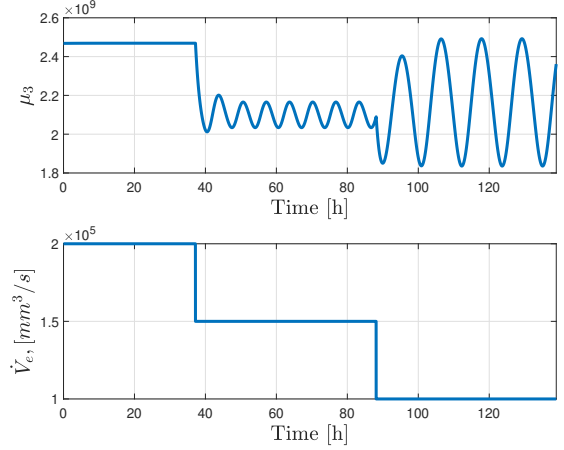$$h = \frac{V}{(1 - \varepsilon)A} = \frac{\pi \int_0^\infty L^3 n dL}{(1 - \varepsilon)A}$$ (7)

Fig. 2. Step response of the third moment μ_3 of the particle size distribution for different injection rates $\dot{V}_e$.

The product withdrawal can be described by a Tromp curve approximation (Rumpf (1990)) with a drain constant K

$$\dot{n}_{prod} = K \frac{\int_0^L exp((L - L_1)^2/(2\sigma_1)) dL}{\int_0^\infty exp((L - L_1)^2/(2\sigma_1)) dL} n.$$ (8)

It represents the probability of particles with size L to be withdrawn from the granulator with respect to the desired classification diameter L_1 and selectivity σ_1.

To simulate the resulting population balance model, a finite volume method with 150 uniform grid points along the particle size coordinate L was used. The parameters were adopted from Vreman et al. (2009), Palis and Kienle (2012b) and are represented in Table 1.

Table 1. Model parameters

$\dot{V}_e$	$1.68 \cdot 10^{-4} m^3/s$	injection rate
ε	0.5	fluidized bed porosity
A	$5 m^2$	granulator cross-sectional area
h_{noz}	$0.44 m$	nozzle height
b_∞	0.028	minimum nucleation rate
L_0	$0.3 mm$	medium diameter of nuclei
σ_0	$0.05 mm$	standard deviation of nuclei diameter
L_1	$0.7 mm$	medium classification diameter
σ_1	$0.05 mm$	classification selectivity
K	$1.92 \cdot 10^{-4} 1/s$	product removable rate

It is well-known and systematically studied, that below a certain injection rate $\dot{V}_e$, limit cycles occur around the steady-state of the particle size distribution (Vreman et al. (2009), Schmidt et al. (2015), Neugebauer et al. (2017)). For the parameters listed above, the system becomes unstable for $\dot{V}_e < 1.7 \cdot 10^5 mm^3/s$, which is also represented in Fig.2.

3. DATA-DRIVEN KOOPMAN SUBSPACE IDENTIFICATION

3.1 Koopman operator theory

Koopman operator theory allows for a linear representation of a nonlinear dynamical system through lifting its

state vector up to higher or in general infinite dimensions. We consider a discrete-time nonlinear system with control input of the following form.

$$x_{k+1} = F(x_k, u_k), \tag{9}$$

Here, x is the state vector, u is the input vector and F is the flow map, that propagates the state vector x forward in time.

Initially the Koopman theory was developed by Koopman (1931) for autonomous systems and later generalized to allow for control inputs (Proctor et al. (2018)). Under the assumption that the control inputs are not dynamically evolving, the system (9) can be lifted up to an infinite-dimensional space, where the dynamics of the system is linear.

$$g(F(x_k, u_k), 0) = \mathcal{K}g(x_k, u_k) \tag{10}$$

Here, $g(\cdot)$ is a nonlinear embedding into an infinite-dimensional space, and $\mathcal{K}$ is the Koopman operator, that linearly propagates the states of the system forward in time.

To allow for Koopman analysis, a finite-dimensional representation of the system is required. Thus, different data-driven methods for Koopman invariant subspace approximations were proposed, like dynamic mode decomposition (DMD) (Tu H. et al. (2014)), (Williams et al. (2015)), kernel-based methods (O. Williams et al. (2015)) and neural networks (Lusch et al. (2018), Takeishi et al. (2017), Yeung E. et al. (2019)).

3.2 Data-driven Koopman subspace identification

The main idea here is to find a finite-dimensional mapping and an approximation of the Koopman operator, that embeds the nonlinear dynamics into a high-dimensional space, where the system behavior is approximately linear. Specifically, we try to identify the nonlinear transformation to the lifted coordinates $z = \phi(x, u)$, along with an appropriate linear system matrix A, input matrix B and output matrix C, such that:

$$z_{k+1} = Az_k + Bu_k. \tag{11}$$
$$y_{k+1} = Cz_{k+1}. \tag{12}$$

For complex nonlinear dynamical systems it is often the case, that not the entire state vector is measurable. In worst case, only the measurements of the controlled output are available. Thus, to capture the dynamics of the system, time delayed vectors of the outputs y and inputs u are constructed

$$X_k = [y_k, y_{k-1}, \ldots y_{k-N}], \tag{13}$$
$$U_k = [u_{k-1}, \ldots u_{k-N}]. \tag{14}$$

To find a respective nonlinear transformation ϕ, a deep neural network is used, which transforms the delayed vectors to the embedded coordinates:

$$z_k = \phi(X_k, U_k). \tag{15}$$

Note, that the delayed vector U_k does not contain the current input value u_k to avoid a nonlinear dependence of intrinsic states z_k from the current input. The overall
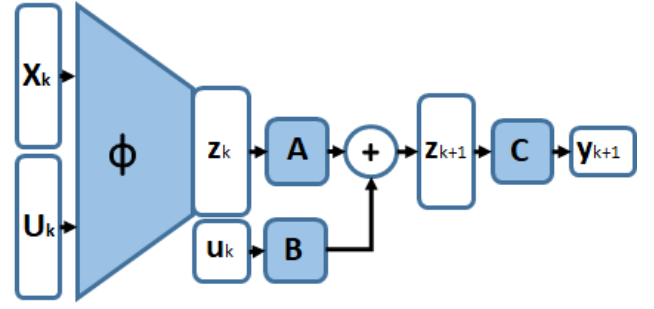

Fig. 3. Structure of Koopman-subspace identification process.

structure of the resulting identification system is shown in Fig.3.

The parameters of the proposed system are found through back-propagation, minimizing the following loss functions:

(1) Embedded space linear output loss, which forces the original output to be a linear combination of the embedded states.

$$\mathcal{L}_{em} = \|y_k - C\phi(X_k, U_k)\|_2^2 \tag{16}$$

(2) Output reconstruction loss, which penalizes the deviation of predicted output from the measured value. To capture long system dynamics, a prediction of M steps is applied, which results in the following loss function.

$$\mathcal{L}_{out} = \sum_{i=1}^{M} \|y_{k+i} - Cz_{k+i}\|_2^2 \tag{17}$$

(3) Embedded space linearity loss, which penalizes the difference between the predicted value and the transformed real measurements:

$$\mathcal{L}_{lin} = \sum_{i=1}^{M} \|\phi(X_{k+i}, U_{k+i}) - z_{k+i}\|_2^2. \tag{18}$$

This loss allows to discover a nonlinear transformation to the embedded coordinates, where the system's dynamic is linear.

The term z_{k+i} in equations (17), (18) is calculated according to (11) in recursive manner. An L_1 regularization is added for matrices A, B, and C during identification procedure, to find a sparse and compact linear system representation:

$$\mathcal{L}_{reg} = \|A\|_1 + \|B\|_1 + \|C\|_1. \tag{19}$$

Thus, the resulting loss function has the following form:

$$\mathcal{L} = \frac{\alpha}{M}(\mathcal{L}_{em} + \mathcal{L}_{out}) + \frac{\beta}{M}\mathcal{L}_{lin} + \gamma\mathcal{L}_{reg} \tag{20}$$

where α, β, γ are scalar weights.

The network uses the generated output trajectories for training. The data from different experiments can be utilized to form a sufficient training set.

3.3 Koopman subspace identification for fluidized bed spray granulation

The presented population balance model is highly nonlinear and can become unstable under certain operating conditions. This leads to oscillations in the resulting particle

size distribution, which is undesired and requires a stabilizing control strategy. Identifying a linear representation of the system would allow for easier controller design, system stabilization, and quality control.

Thus, to derive a linearized model of the system, the volume flow rate $\dot{V}_e$ is chosen as an actuated variable

$$u = \dot{V}_e. \tag{21}$$

The third moment of the particle size distribution is used as the controlled output value, since it is correlated with the bed mass and can be derived from pressure measurements

$$y = \mu_3. \tag{22}$$

Using the randomly generated input values, the corresponding particle size distribution is calculated, using the population balance model (1). After calculation of the third moment of the distribution, the delayed vectors U_k and X_k are composed, using a sampling time $t_s = 60s$.

The neural network consists of 4 fully-connected layers with ReLU nonlinearity. The number of inputs and outputs for each layer is set to be 2N-1 $\xrightarrow{\text{layer1}}$ N $\xrightarrow{\text{layer2}}$ N/2 $\xrightarrow{\text{layer3}}$ N/4 $\xrightarrow{\text{layer4}}$ L respectively, where N is the length of delayed vector and L is the dimension of the embedded coordinates. The layer parameters were initialized according to Gaussian distribution. The matrices A, B, and C were initialized as a solution to the following linear system, using Moore-Penrose inverse:

$$\begin{bmatrix} z_{k+1} \\ y_{k+1} \end{bmatrix} = \begin{bmatrix} A & B \\ C & 0 \end{bmatrix} \begin{bmatrix} z_k \\ u_k \end{bmatrix} \tag{23}$$

For loss minimization, an Adam optimizer was used. The values of the hyperparameters are shown in Table 2.

Table 2. Training parameters

N	60	length of the delayed vectors
M	30	number of prediction steps
L	10	dimension of the embedded state z
α	1	output loss weight
β	1	linearity loss weight
γ	10^{-6}	L_1 regularization weight
η	10^{-3}	learning rate

The training data was scaled to the range [0,1]. The initial conditions of the system were set to a stable region with a particle size distribution, that corresponds to the injection rate $\dot{V}_e = 2 \cdot 10^5 mm^3/s$. The resulting input/output trajectories, as well as their reconstructions are shown in Fig. 4.

4. CONTROLLER DESIGN

The complex and nonlinear nature of the fluidized bed spray granulation process makes controller design a challenging task. Although, a number of different model control approaches (Bück et al. (2016); Palis and Kienle (2012b, 2014)) have been proposed, their performance heavily depends on the model accuracy.

Using the data-driven Koopman-linearized system model, a conventional linear quadratic control with integral action
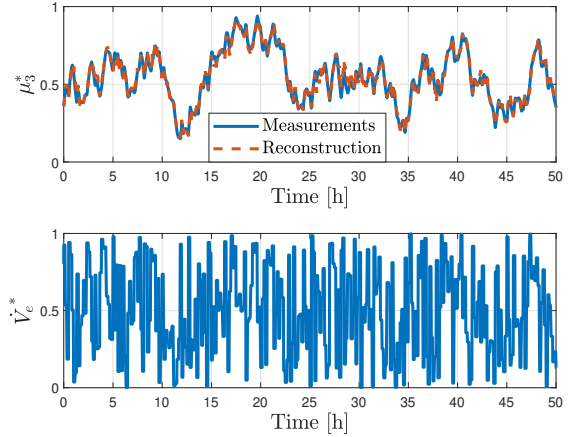

Fig. 4. Training trajectories with reconstructed values of normalized third moment μ_3 and corresponding scaled uniform random input value $\dot{V}_e$ used for system identification.

(LQI) can be designed. After augmenting the system with the integrating sum of the output error

$$\tilde{z}_k = \begin{bmatrix} z_k \\ \varepsilon_k \end{bmatrix} = \begin{bmatrix} z_k \\ \sum_{i=0}^{k} (r_i - y_i) t_s \end{bmatrix}, \tag{24}$$

where r is the desired set-point and y is the controlled output of the plant, the gain vector K can be found by solving the following discrete linear quadratic minimization problem

$$J = \sum_{k=0}^{\infty} (\tilde{z}_k^T Q \tilde{z}_k + u_k^T R u_k). \tag{25}$$

Here, Q and R are state and input weighting matrices and $\tilde{z}_k$ is the augmented state vector.

Since according to (12), the measured output is a linear combination of the embedded states z, a linear full-rank transformation T can be found, such that:

$$y_k = [1, 0, \ldots, 0] T z_k. \tag{26}$$

Thus, the resulting feedback control can be decomposed in the following parts:

$$u_k = -K_i \varepsilon_k - K_{lin} y_k - K_{nonlin} \phi(X_k, U_k), \tag{27}$$

which contains an integral action, linear system output feedback, and nonlinear states feedback. Fig.5 shows the resulting structure of the proposed LQI control.

4.1 Results

The proposed control strategy was implemented in Matlab together with the granulation process simulation and the neural network feed-forward calculation. The constant feedback gains are calculated once for a diagonal matrix Q that mainly penalizes the linear output and error states with value 1, and R is set to 5000 to limit the input signal.

Fig. 6 shows the resulting dynamics of controlled system in the stable region. The proposed controller was able to improve the dynamical performance during the step response, compared to the open-loop system.
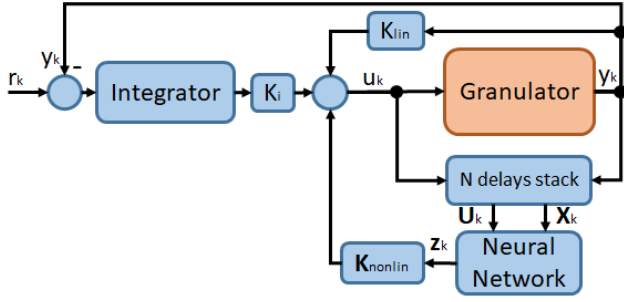
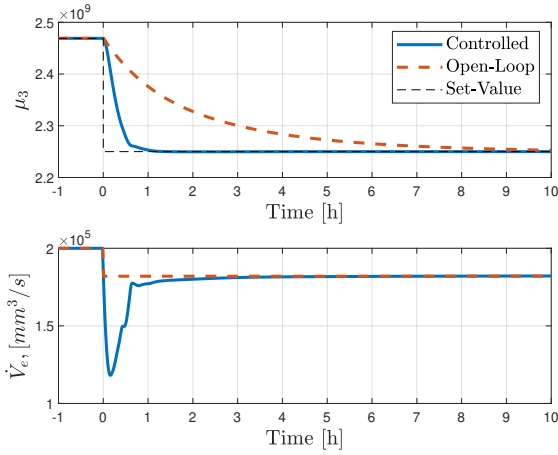Fig. 5. Resulting structure of the proposed LQI-Koopman control.

Fig. 6. Step response from the stable region into the unstable for the controlled and open-loop system.

Since Koopman linearization does not depend on any linearization point, no parameter adaptation is needed for different operational regimes. Fig. 7 shows the resulting system response for a step input from the stable region with injection rate $\dot{V}_e = 2 \cdot 10^5\ mm^3/s$ into the unstable region with $\dot{V}_e = 1.4 \cdot 10^5\ mm^3/s$. Despite the difference in the operating point, the proposed control system is able to stabilize the output without degradation in the dynamical performance of the system. The stabilization of the third moment also results in a stable particle size distribution, as shown in Fig. 8, 9.

5. CONCLUSION

In this paper, a purely data-driven approach for the control of a fluidized bed spray granulation process was proposed, that does not require any prior model knowledge. Based on the Koopman operator theory, a finite-dimensional Koopman-invariant subspace was approximated with deep neural networks. A nonlinear transformation was found, that maps the states of the nonlinear system to the embedded coordinates, where the dynamics of the system is approximately linear. This allows for system linearization, that does not depend on an operating point. Based on the Koopman-linearized coordinates, an LQI controller was designed. It was shown, that the proposed controller can successfully stabilize the particle size distribution and does not depend on the operating point. Thus, it can be used
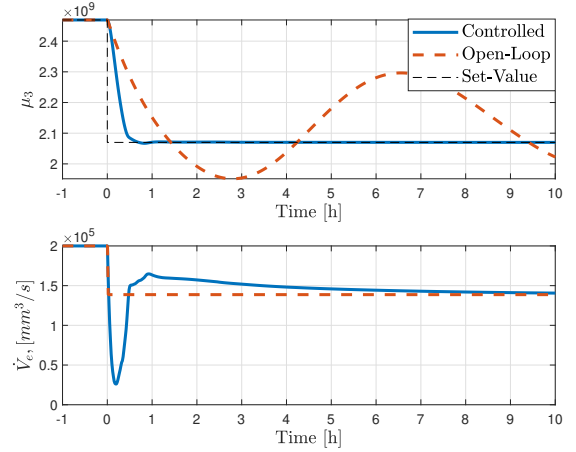

Fig. 7. Step response from the stable region into the unstable for the controlled and open-loop system.
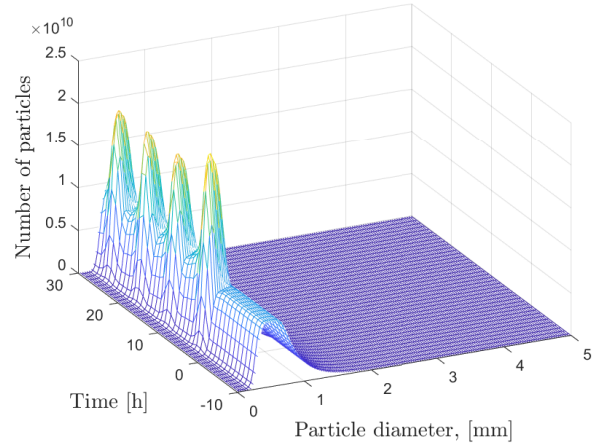

Fig. 8. Particle size distribution for a step response from the stable into the unstable region without control.
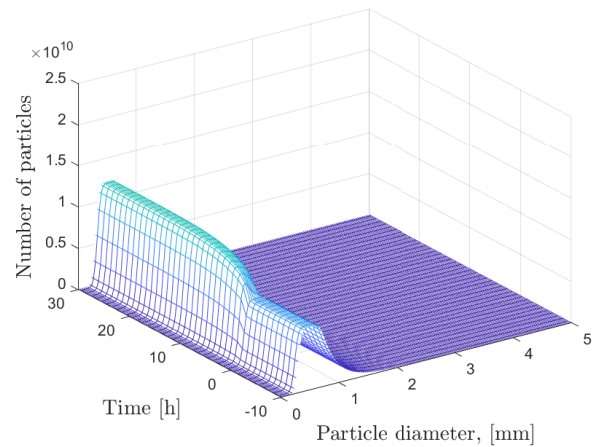

Fig. 9. Particle size distribution for a step response from the stable into the unstable region for the controlled system.

for different regimes of the granulation process, without any parameter adjustment.

REFERENCES

Brunton, S.L., Brunton, B.W., Proctor, J.L., and Kutz, J.N. (2016). Koopman invariant subspaces and finite linear representations of nonlinear dynamical systems for control. *PLOS ONE*, 11(2), 1–19.

Bück, A., Dürr, R., Schmidt, M., and Tsotsas, E. (2016). Model predictive control of continuous layering granulation in fluidised beds with internal product classification. *Journal of Process Control*, 45, 65–75.

Kaiser, E., Kutz, J.N., and Brunton, S. (2017). Data-driven discovery of koopman eigenfunctions for control. *arXiv: Optimization and Control*.

Koopman, B.O. (1931). Hamiltonian systems and transformation in hilbert space. *Proceedings of the National Academy of Sciences of the United States of America*, 17(5), 315–318.

Korda, M. and Mezić, I. (2018). Linear predictors for nonlinear dynamical systems: Koopman operator meets model predictive control. *Automatica*, 93, 149–160.

Lusch, B., Kutz, J.N., and Brunton, S.L. (2018). Deep learning for universal linear embeddings of nonlinear dynamics. *Nature Communications*, 9(1), 851.

Maksakov, A. and Palis, S. (2020). Koopman-based optimal control of boost dc-dc converter. In *2020 IEEE Problems of Automated Electrodrive. Theory and Practice (PAEP)*, 1–4. IEEE.

Mauroy, A., Mezić, I., and Susuki, Y. (2020). *The Koopman Operator in Systems and Control*, volume 484. Springer International Publishing, Cham.

Narasingam, A. and Kwon, J.S.I. (2019). Koopman lyapunov–based model predictive control of nonlinear chemical process systems. *AIChE Journal*, 65(11), 1.

Neugebauer, C., Palis, S., Bück, A., Tsotsas, E., Heinrich, S., and Kienle, A. (2017). A dynamic two-zone model of continuous fluidized bed layering granulation with internal product classification. *Particuology*, 31, 8–14.

O. Williams, M., W. Rowley, C., and G. Kevrekidis, I. (2015). A kernel-based method for data-driven koopman spectral analysis. *Journal of Computational Dynamics*, 2(2), 247–265.

Palis, S. and Kienle, A. (2012a). Discrepancy based control of continuous fluidized bed spray granulation with internal product classification. In *8th International Symposium on Advanced Control of Chemical Processes, ADCHEM 2012*, 756–761. IFAC.

Palis, S. and Kienle, A. (2012b). H∞ loop shaping control for continuous fluidized bed spray granulation with internal product classification. *Industrial & Engineering Chemistry Research*.

Palis, S. and Kienle, A. (2014). Discrepancy based control of particulate processes. *Journal of Process Control*, 33–46.

Proctor, J.L., Brunton, S.L., and Kutz, J.N. (2018). Generalizing koopman theory to allow for inputs and control. *SIAM Journal on Applied Dynamical Systems*, 17(1), 909–930.

Randolph, A.D. and Larson, M.A. (1971). *Theory of particulate processes: Analysis of techniques of continuous crystallization*. Acad. Press, New York, NY.

Rumpf, H. (1990). *Particle technology*. Powder technology series. Chapman and Hall, London.

Schmidt, M., Bück, A., and Tsotsas, E. (2015). Experimental investigation of process stability of continuous spray fluidized bed layering with internal separation. *Chemical Engineering Science*, 126, 55–66.

Takeishi, N., Kawahara, Y., and Yairi, T. (2017). Learning koopman invariant subspaces for dynamic mode decomposition. In *Proceedings of the 31st International Conference on Neural Information Processing Systems*, NIPS'17, 1130–1140. Curran Associates Inc., Red Hook, NY, USA.

Tu H., J., Rowley W., C., Luchtenburg M., D., L. Brunton, S., and Nathan Kutz, J. (2014). On dynamic mode decomposition: Theory and applications. *Journal of Computational Dynamics*, 1(2), 391–421.

Vreman, A.W., van Lare, C.E., and Hounslow, M.J. (2009). A basic population balance model for fluid bed spray granulation. *Chemical Engineering Science*, 64(21), 4389–4398.

Williams, M.O., Kevrekidis, I.G., and Rowley, C.W. (2015). A data–driven approximation of the koopman operator: Extending dynamic mode decomposition. *Journal of Nonlinear Science*, 25(6), 1307–1346.

Yeung E., Kundu S., and Hodas N. (2019). Learning deep neural network representations for koopman operators of nonlinear dynamical systems. In *2019 American Control Conference (ACC)*, 4832–4839.